

Pixel-to-pixel variation on a calibrated PILATUS3-based multi-energy soft x-ray detector

P. VanMeter, L. F. Delgado-Aparicio, L. Reusch, N. Pablant, J. Maddox, M. Rissi, B. Luethi, T. Donath, C. Schulze-Briese, K. Hill, and D. Den Hartog

Citation: [Review of Scientific Instruments](#) **89**, 10G119 (2018); doi: 10.1063/1.5037347

View online: <https://doi.org/10.1063/1.5037347>

View Table of Contents: <http://aip.scitation.org/toc/rsi/89/10>

Published by the [American Institute of Physics](#)

Articles you may be interested in

[Simulation, design, and first test of a multi-energy soft x-ray \(SXR\) pinhole camera in the Madison Symmetric Torus \(MST\)](#)

[Review of Scientific Instruments](#) **89**, 10G116 (2018); 10.1063/1.5038798

[A computational tool for simulation and design of tangential multi-energy soft x-ray pin-hole cameras for tokamak plasmas](#)

[Review of Scientific Instruments](#) **89**, 10G120 (2018); 10.1063/1.5038788

[The single-line-of-sight, time-resolved x-ray imager diagnostic on OMEGA](#)

[Review of Scientific Instruments](#) **89**, 10G117 (2018); 10.1063/1.5036767

[A new toroidal x-ray crystal spectrometer for the diagnosis of high energy density plasmas at the National Ignition Facility](#)

[Review of Scientific Instruments](#) **89**, 10F118 (2018); 10.1063/1.5036806

[Liquid crystal polymer receiver modules for electron cyclotron emission imaging on the DIII-D tokamak](#)

[Review of Scientific Instruments](#) **89**, 10H120 (2018); 10.1063/1.5035373

[On the system stability and calibration of the image plate/scanner system for plasma diagnosis at the National Ignition Facility](#)

[Review of Scientific Instruments](#) **89**, 10F123 (2018); 10.1063/1.5039363



Nanopositioning Systems Micropositioning AFM & SPM Single molecule imaging

Pixel-to-pixel variation on a calibrated PILATUS3-based multi-energy soft x-ray detector

P. VanMeter,^{1,a)} L. F. Delgado-Aparicio,² L. Reusch,¹ N. Pablant,² J. Maddox,³ M. Rissi,⁴ B. Luethi,⁴ T. Donath,⁴ C. Schulze-Briese,⁴ K. Hill,² and D. Den Hartog¹

¹Department of Physics, University of Wisconsin-Madison, Madison, Wisconsin 53706, USA

²Princeton Plasma Physics Laboratory (PPPL), Princeton, New Jersey 08540, USA

³Department of Engineering Physics, University of Wisconsin-Madison, Madison, Wisconsin 53706, USA

⁴DECTRIS Ltd., 5405 Baden-Dättwil, Switzerland

(Presented 17 April 2018; received 23 April 2018; accepted 4 June 2018; published online 10 October 2018)

A multi-energy soft x-ray pin-hole camera based on the PILATUS3 100 K x-ray detector has recently been installed on the Madison Symmetric Torus. This photon-counting detector consists of a two-dimensional array of $\sim 100\,000$ pixels for which the photon lower-threshold cutoff energy E_c can be independently set for each pixel. This capability allows the measurement of plasma x-ray emissivity in multiple energy ranges with a unique combination of spatial and spectral resolution and the inference of a variety of important plasma properties (e.g., T_e , n_Z , Z_{eff}). The energy dependence of each pixel is calibrated for the 1.6–6 keV range by scanning individual trimbit settings, while the detector is exposed to fluorescence emission from Ag, In, Mo, Ti, V, and Zr targets. The resulting data for each line are then fit to a characteristic “S-curve” which determines the mapping between the 64 possible trimbit settings for each pixel. The statistical variation of this calibration from pixel-to-pixel was explored, and it was found that the discreteness of trimbit settings results in an effective threshold resolution of $\Delta E < 100$ eV. A separate calibration was performed for the 4–14 keV range, with a resolution of $\Delta E < 200$ eV. Published by AIP Publishing. <https://doi.org/10.1063/1.5037347>

I. INTRODUCTION

The multi-energy soft x-ray (ME-SXR) diagnostic system at the Madison Symmetric Torus (MST) has been developed as a collaboration between the University of Wisconsin-Madison Department of Physics and PPPL. The diagnostic is based around a novel implementation of the PILATUS3 100k detector which has been calibrated to simultaneously sample the plasma emission at multiple x-ray energy ranges. This provides sensitivity to a variety of important plasma properties such as core T_e and n_e , as well as impurity species content.¹

The PILATUS3 detector was calibrated for multi-energy operation, following a procedure developed for the PILATUS2 detector at Alcator C-Mod² and later extended to the PILATUS3.³ This paper builds upon this prior work by applying this procedure to a new system and then using the results to analyze pixel to pixel variation across the detector. Of particular interest was the resolution to which a specific photon energy threshold could be set due to uncertainty in the calibration procedure and the discrete nature of the PILATUS3 threshold settings. This resolution was found to be $\Delta E < 100$ eV for a 1.6–6 keV calibration and $\Delta E < 200$ eV for a 4–14 keV calibration. These results are discussed in Secs. II and III, respectively.

A brief introduction to the PILATUS3 detector itself is provided in Sec. I A, and an overview of the energy calibration

technique is provided in Sec. I B. A discussion of the design, implementation, and simulation of the ME-SXR diagnostic at MST is presented as a separate contribution to these proceedings.⁴

A. The PILATUS3 detector

The PILATUS3 100k detector is a photon-counting pixelated x-ray detector produced commercially by DECTRIS Ltd. The device is composed of a single $450\ \mu\text{m}$ Si sensor which absorbs incident photons and converts them to a cloud of charge.⁵ This charge is then transferred via a bump-bonded indium connection to one of the many charge-sensitive preamplifiers (CSA) located on one of the 16 application-specific integrated circuits (ASICs) that compose the detector. The charge is converted to a pulse which is discriminated against a threshold by a comparator, rejecting photons with energies below the threshold. The threshold is controlled by a global V_{cmp} setting but can be further adjusted, or trimmed, on an individual level by an additional setting stored in a 6-bit register called the “trimbit” setting. Pulses that pass this threshold are recorded into a 20-bit counter and read out at pre-set intervals. These ASICs are arranged in an 8×2 grid, each contain an array of 60×97 individual pixels (each with its own CSA, comparator, trimbit setting, and counter), leading to a total of $480 \times 194 = 93\,120$ pixels (often referred to as 100k).

The individual trimbit settings exist to permit the detector to compensate for inhomogeneities resulting from the manufacturing process and achieve a uniform photon energy threshold, which is the intent of the standard factory calibration.

Note: Paper published as part of the Proceedings of the 22nd Topical Conference on High-Temperature Plasma Diagnostics, San Diego, California, April 2018.

^{a)}Electronic mail: pvanmeter@wisc.edu

The ME-SXR concept, however, uses a custom calibration to take advantage of the trimbit settings in order to intentionally set different energy thresholds for pixels across the detector. This allows the implementation of custom configurations which combine spatial and spectral resolution into a single diagnostic which can be quickly and easily configured for a specific scientific goal.

Global settings determine the minimum energy threshold (V_{cmp}), gain (V_{rf}), and extent of individual trimbit increments on the energy threshold (V_{trm}). Appropriate global settings were determined which permitted sensitivity to multiple energy ranges of interest. Then the calibration procedure which is the subject of the rest of this paper was applied to determine the mapping between the trimbit setting and the energy threshold E_c for each individual pixel. Two specific energy-range calibrations are discussed here: a 1.6–6 keV calibration (Sec. II) and a 4–14 keV calibration (Sec. III).

B. Energy calibration technique

The goal of the energy calibration is to determine for each pixel the mapping between the trimbit register setting and its corresponding photon cutoff energy threshold, E_c .³ Data for the energy calibration were collected at the DECTRIS facility in Switzerland. The detector module was exposed to a nearly uniform x-ray source generated by fluorescence. Once the appropriate global settings were determined and exposure was taken with each pixel's trimbit value set to $\hat{t} = 0$. This exposure was then repeated with all trimbits set to $\hat{t} = 1, 2, \dots, 63$. The data of this trimbit scan have a characteristic S-curve shape,² as shown in Fig. 1. This curve is well described by the equation

$$N(\hat{t}) = \frac{1}{2} \left[\operatorname{erf}\left(-\frac{\hat{t} - a_0}{a_1 \sqrt{2}}\right) + 1 \right] \left(a_2 + a_3(\hat{t} - a_0) \right) + a_4 + a_5(\hat{t} - a_0), \quad (1)$$

where \hat{t} is the trimbit setting, here allowing us to assume non-integer values, a_0 is the location of the S-curve inflection point, a_1 is the width of the error function (corresponding to the standard deviation of the integrated Gaussian), a_2 is the signal level, a_3 is the slope of a linear distortion due to charge-sharing

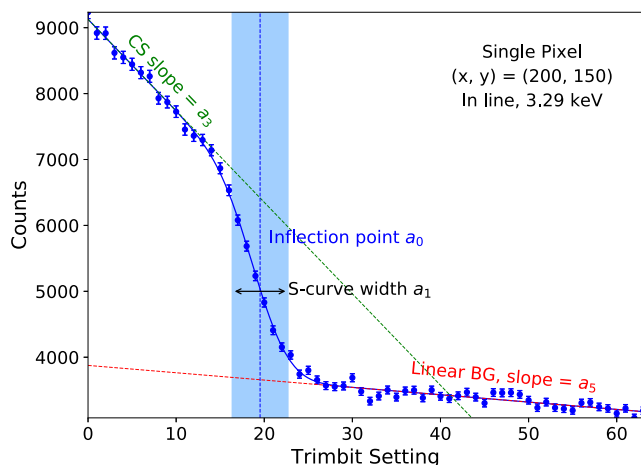


FIG. 1. The trimbit scan calibration S-curve for a single pixel exposed to the indium line at 3.29 keV. Key features of the curve are annotated as they relate to Eq. (1).

(CS) by adjacent pixels,⁶ and a_4 and a_5 describe a linear offset due to the background signal (BG). The relation between these fit terms and the S-curve shape is illustrated by Fig. 1.

The term a_0 describes the trimbit value which sets E_c for that specific pixel to the energy of the source photons. This value was obtained for each pixel by performing a nonlinear fit of the trimbit scan data to Eq. (1). A mapping between the trimbit setting and E_c was generated for each pixel by repeating this procedure for XRF sources with emission lines at different energies within the desired calibration range. This mapping is well described by a quadratic polynomial, so for each pixel a fit was performed in order to allow interpolation between calibration energies. The uncertainty in the fit was also estimated, accounting for correlations in the fit parameters.

II. 1.6–6 keV CALIBRATION RESULTS

The detector global settings were configured with a threshold of under 2 keV up to just more than 6 keV, and a calibration was performed following the procedure outlined above using fluorescent Zr, Mo, Ag, In, Ti, and V targets with energies ranging between 2 and 5 keV (see Fig. 2). This range is of interest on MST in order to diagnose the strong Al^{11+} and Al^{12+} lines which are observed between 1.6 and 2 keV,⁷ as well as to provide continuum T_e measurements.

A. Overview of fit results

The calibration procedure described in Sec. I B was performed individually for each of the $\sim 100\text{k}$ pixels on the detector. The resulting S-curves for an example pixel are shown in Fig. 2, with linear background removed for the purpose of illustration. The detector counts have also been normalized so that the response is equal to one when the threshold is at half of the incident photon energy. The fit values a_0 are then used to generate a trimbit- E_c curve, as shown in Fig. 3. These mappings allow for the implementation of custom E_c configurations within this sensitivity range.

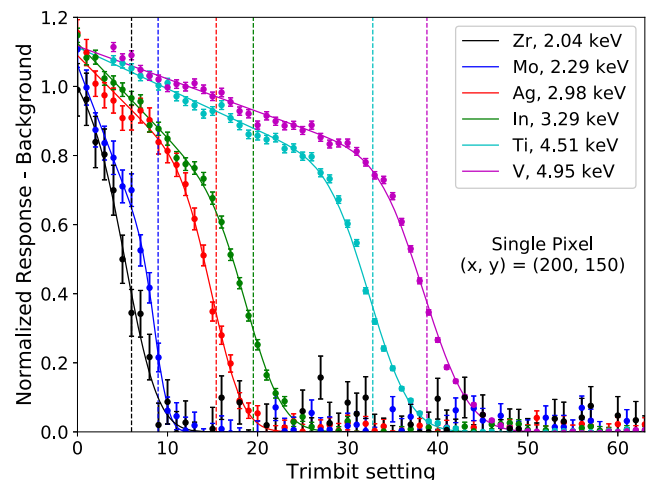


FIG. 2. All trimbit scan calibration S-curves for a single pixel. For this plot, the linear background was subtracted off and the signal level was normalized. The dashed lines indicate the location of the inflection points a_0 . Uncertainties in the individual counts were assumed to follow Poisson statistics.

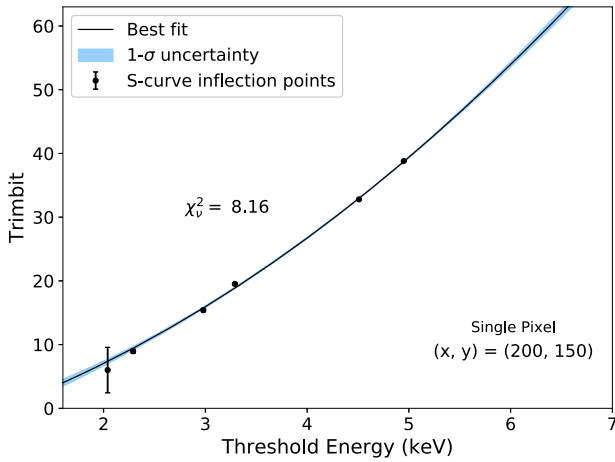


FIG. 3. Single pixel inflection point a_0 data fit to a quadratic curve with the resulting 1σ uncertainty region highlighted. The uncertainty in the a_0 values, indicated by the black error bars, was taken from the variance in the S-curve fits. The shape of the fit and level of uncertainty is typical of all pixels across the detector.

The calibration data were sufficient to well characterize the mapping, as demonstrated by the small region of uncertainty surrounding the fit values in Fig. 3. It is notable that the uncertainty in the trimbit- E_c mapping for any given individual pixel is much smaller than the variation between pixels across the detector.

B. Pixel-to-pixel variation of the calibration

Substantial correlated variation in the results of the energy calibration was observed across the detector’s $\sim 100k$ pixels. This variation can be seen in Fig. 4, which shows the trimbit- E_c mappings for 500 randomly selected pixels, demonstrating a variation of the order of 10 trimbits to achieve the same energy threshold. The standard deviation of the inflection point a_0 was found to be significantly larger for the 2.04 keV Zr. This is because the S-curve threshold for this line was near the lower-limit of the detectors sensitivity, meaning that the algorithm

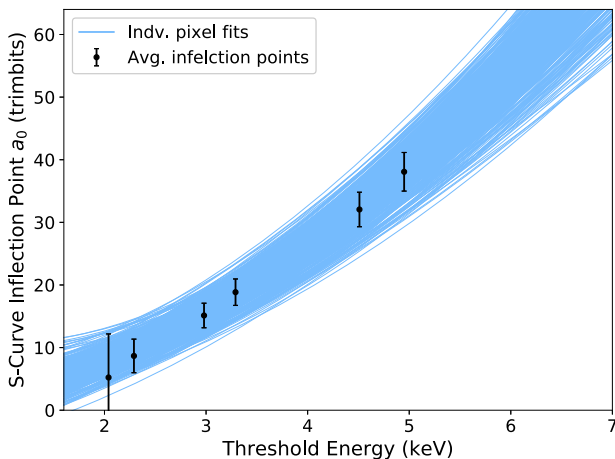


FIG. 4. The blue lines show the trimbit- E_c mapping for 500 randomly selected pixels, showing a spread of ~ 10 trimbits for a given threshold. The black points show the average trimbit setting of the S-curve inflection point for each X-ray source, and the error bars show the standard deviation.

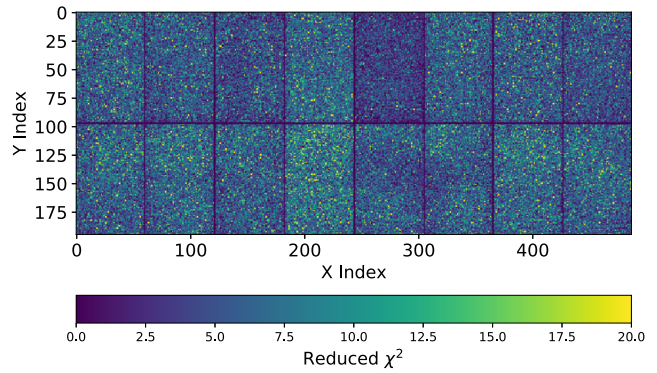


FIG. 5. Map of the reduced χ^2 for the quadratic trimbit- E_c fit for each pixel. The columns and rows between the rectangular chips do not collect data and have thus been zeroed out.

sometimes struggled to determine where the S-curve flattened out at the top. This uncertainty was accounted for in the fit with larger error-bars.

The quality of the trimbit- E_c fit was explored by calculating $\chi^2 = \sum_s (a_{0,s} - \hat{i}(E_{c,s}))^2 / \sigma_s^2$ for each pixel, where s labels each X-ray source, $E_{c,s}$ is the X-ray line energy of that source, and $\hat{i}(E_c)$ is the best-fit quadratic trimbit- E_c mapping. As shown in Fig. 5, this was found to be relatively uniform across the detector, though some correlation between pixels on the same ASIC can be observed.

Multiple trimbit configurations were produced which each set a uniform threshold across the detector ranging from 1.8 keV to 6.3 keV in order to investigate how the variation between pixels affects energy resolution. For each energy, the trimbit- E_c calibration was used to determine the exact trimbit value which would be required to set each pixel to that particular energy threshold, permitting non-integer values. The distribution of these trimbit settings, shown in Fig. 6, is well described as normal. The distribution is seen to widen as the desired threshold energy is increased, with a standard deviation varying from less than 2 trimbits to more than 4. This plot also shows the limits of this calibration’s energy range, as threshold settings above 6.0 keV result in an appreciable

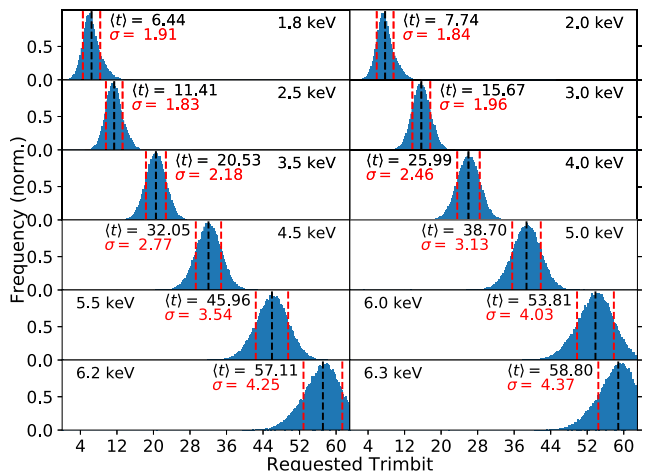


FIG. 6. Distribution of trimbit settings required to set the detector to the specified uniform threshold. These values must be rounded to the nearest integer before the detector can be configured.

number of pixels requiring a trimbit setting above the hardware limit of 63.

C. Effect of pixel-to-pixel variation on energy resolution

For an appropriate ME-configuration of the detector, the trimbit settings obtained from the calibration must be rounded to the nearest integer value. As a result of this rounding, all pixels in a particular row or column will actually be set to slightly different thresholds within the range $E_c \pm \Delta E$. The value ΔE therefore serves as the limitation on the resolution of the detector under this calibration.

The value of ΔE was determined by taking the pixel trimbit settings for each of the uniform configurations as shown in Fig. 6, rounding them to the nearest integer value, and then mapping the resultant integer back to its corresponding energy threshold using the calibrated trimbit- E_c mapping, of the type shown in Fig. 3. The resulting distributions shown in Fig. 7 are nearly uniform with sloped edges. This uniformity is a result of the fact that the variation between pixels is arbitrary and no particular trimbit- E_c mapping is preferred. The slopes at the edge of the distribution are a result of uncertainty in the calibration procedure. The largest values of ΔE are seen at low specified E_c , where the trimbit- E_c mapping is the least steep. For all energies within the range of this calibration, the threshold can be set with a resolution of less than 100 eV.

Since this analysis depends on the assumption that the trimbit- E_c mappings produced by the calibration procedure are essentially correct, it is worthwhile to quantify the level of uncertainty in the calibration results at each considered energy threshold. This was determined by making a histogram of the calibration uncertainty associated with each pixel. For the pixel shown in Fig. 3, for instance, this is the size of the blue shaded region evaluated at the appropriate trimbit. The results, displayed in Fig. 8, show an uncertainty of about the same size as ΔE for low threshold settings but that becomes minimal

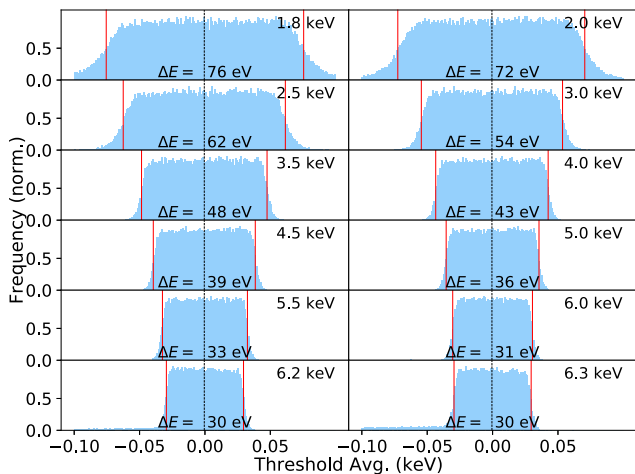


FIG. 7. Distribution of energy thresholds $\Delta E - \langle \Delta E \rangle$ across all pixels given a common target threshold resulting from discrete trimbit settings. The distribution is observed to be nearly uniform, with ΔE ranging from 30 to 76 eV depending on the requested threshold.

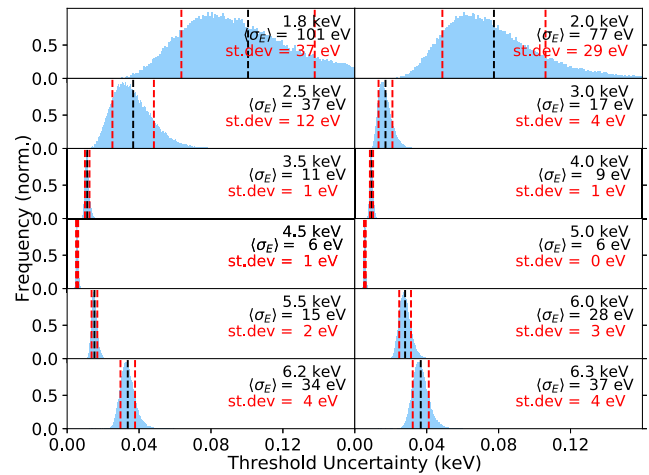


FIG. 8. Uncertainty in the threshold energy resulting from Poisson uncertainty propagating through the calibration procedure. This uncertainty is seen to be substantially smaller than the threshold variation ΔE due to rounding for threshold settings of ~ 3 keV and larger. Note that since the distribution is somewhat skewed toward high uncertainty, the mean and mode of a given distribution do not exactly agree.

by a threshold of about 3.0 keV. This explains the sloping feature on the edges of the low-threshold uniform distributions in Fig. 7.

Another consideration for describing the resolution of the detector is the width of the S-curve, described by the parameter a_1 in Eq. (1). This parameter characterizes the width of the region between which the detector transmission, also described by an S-curve,¹ increases from 0 to 1 so that any photons within this energy range have a fractional chance of being counted. Figure 9 shows the average width for all pixels in the data set at each of the calibration line energies. Here the width is presented in terms of a full width at half maximum, $FWHM = 2\sqrt{2 \ln 2} \cdot a_1 \cdot \frac{\partial E_c}{\partial i}$. This plot also shows the S-curve width for 1000 randomly selected pixels. A higher variance in the FWHM is seen in the lower-energy datasets, attributable to the difficulty in performing the S-curve fits when the inflection point is near the detector's lower-energy limit. The S-curve

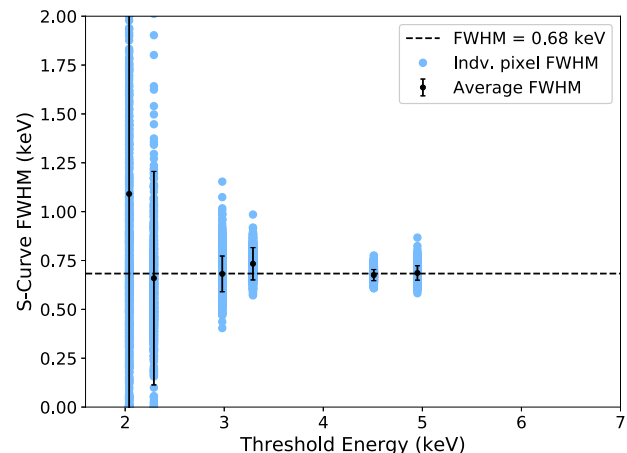


FIG. 9. On average, the width of the S-curves for the 1.6–6 keV calibration is well described as a constant of ~ 0.7 keV. The light blue points represent the width for 1000 randomly selected pixels. The black points are the average of the entire detector, and the error bars are the standard deviations.

width was found to be independent of the energy threshold on average, with a $FWHM \approx 0.7$ keV. This does vary between pixels, and it was observed that a_0 and a_1 tend to be positively correlated.

III. 4–14 keV CALIBRATION RESULTS

This calibration procedure was also performed with global settings chosen for threshold ranges from 4 keV to above 12 keV. This calibration used emission lines from fluoresced Cr, Fe, Cu, Ge, and Br sources at 5.41, 6.40, 8.05, 9.89, and 11.92 keV, respectively.

The level of pixel-to-pixel variation in the trimbit- E_c mapping was found to be consistent with that seen in the 1.6–6 keV calibration. ΔE ranges from approximately 70–200 eV, an increase of about 2.5 times over the 1.6–6 keV calibration. This is consistent with the overall increase energy range covered by the calibration. The uncertainty in the threshold energy resulting from propagated counting error was found to be smaller than ΔE by a factor of 3 or more (depending on the threshold chosen). The scalings of ΔE with threshold setting for both calibrations are shown in Fig. 10. Quadratic fits are also provided for interpolation. S-curves were found to

have a $FWHM \approx 1.3$ keV which was independent of threshold energy.

IV. CONCLUSIONS

The ME-SXR diagnostic at MST, based on the PILATUS3 detector, has been calibrated to sample the x-ray spectrum of the plasma using multiple energy thresholds either between 1.6 and 6 keV or between 4 and 14 keV. Variation in the calibration across all pixels was characterized, with a standard deviation of 2–4 trimbits for a specified E_c . The requirement that the trimbit setting must be an integer resulted in a pixel-to-pixel threshold deviation of $\Delta E < 100$ eV for the 1.6–6 keV calibration and $\Delta E < 200$ eV for the 4–14 keV calibration. In both cases, this variation is either comparable to or smaller than the uncertainty in the calibration results. The S-curves were found to have widths of ~ 0.7 keV and ~ 1.3 keV, respectively.

SUPPLEMENTARY MATERIAL

See [supplementary material](#) for all data shown in the above figures, which is available online.

ACKNOWLEDGMENTS

This material is based upon work supported by the U.S. Department of Energy Office of Science, Office of Fusion Energy Sciences program under Award Nos. DE-SC0015474 and DE-FC02-05ER54814.

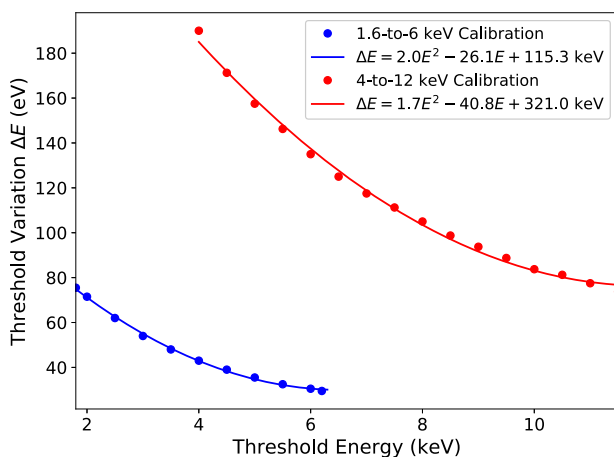


FIG. 10. Threshold variation ΔE vs threshold energy for both the 1.6–6 and 4–14 keV calibrations. Points were calculated using uniform threshold configurations (as in Fig. 7) and interpolated via quadratic fit.

¹L. F. Delgado-Aparicio, J. Maddox, N. Pablant *et al.*, *Rev. Sci. Instrum.* **87**, 11E204 (2016).

²N. Pablant, L. F. Delgado-Aparicio, M. Bitter *et al.*, *Rev. Sci. Instrum.* **83**, 10E526 (2012).

³J. Maddox, N. Pablant, P. Efthimion *et al.*, *Rev. Sci. Instrum.* **87**, 11E320 (2016).

⁴L. F. Delgado-Aparicio, J. Wallace, H. Yamazaki *et al.*, “Simulation, design and first test of a multi-energy soft x-ray (SXR) pinhole camera in the Madison Symmetric Torus (MST),” *Rev. Sci. Instrum.* (these proceedings).

⁵P. Kraft, A. Bergamaschi, Ch. Bröennimann *et al.*, *IEEE Trans. Nucl. Sci.* **56**, 758 (2014).

⁶P. Kraft, A. Bergamaschi, Ch. Bröennimann *et al.*, *J. Synchrotron Radiat.* **16**, 368 (2009).

⁷L. M. Reusch, D. J. Den Hartog, P. Franz *et al.*, *Rev. Sci. Instrum.* **87**, 11E332 (2016).